Journal of Sound and Vibration 330 (2011) 685–702

Contents lists available at ScienceDirect

Journal of Sound and Vibration

journal homepage: www.elsevier.com/locate/jsvi

Vibration of thin, tensioned, helically wrapped plates

Ernesto Lopez, Sinan Müftü *

Northeastern University, Department of Mechanical Engineering, Boston, MA 02115, USA

ARTICLE INFO

Article history:
Received 6 September 2009
Received in revised form
30 August 2010
Accepted 31 August 2010
Handling Editor: S. Ilanko
Available online 20 September 2010

ABSTRACT

Free vibration analysis of a thin tensioned plate, wrapped around a cylindrical guide in a helical manner is presented. The system is a model of a thin, flexible web wrapped around a turn-bar. The equation of motion of the wrapped plate is derived by using the energy method and with the Kirchhoff–Love assumptions. The weak form of the equation of motion was obtained by the finite element method and the eigenvalue problem was solved numerically. The effects of parameters such as plate tension, guide radius, longitudinal and helical wrap angles, plate width, and the lengths of the non-wrapped segments were investigated. Eigenmodes with same mode numbers were observed in symmetric and anti-symmetric fashion about the center of the plate, for symmetrically wrapped plates. It was shown that the plate/shell boundary of the wrapped plate effectively acts like a support. For non-helically wrapped plates the free edges cause a frequency clustering of the lateral modes about the dominant longitudinal mode. The frequency clustering diminishes when helical wrap is introduced.

1. Introduction

Thin materials known as webs are used in the manufacturing of newsprint, thin foils and other similarly thin materials. During manufacturing a web is subjected to various mechanical, thermal and chemical processes depending on the end product. Typically, guides and rollers are used to change the running direction of the web. However, at certain process locations on its path, the web cannot be supported by rollers to change its direction, as contact could damage the product. A *turn-bar*, which is a hollow, pressurized cylindrical drum, is then used to float the web, and to change its direction (Fig. 1) [1]. The web is wrapped around a turn-bar in a helical fashion. The circumferential (θ) and helical (β) components of the wrap, shown in Fig. 1b, change the running direction of the web in the circumferential and axial directions of the turn-bar, respectively. The use of a turn-bar allows versatility in manufacturing floor layout.

The fluid–structure interaction between a web and the air cushion provided by an air reverser (β=0) was studied by Müftü and Cole [2]. The governing equations of the web were coupled to a modified form of the Navier–Stokes equations at steady state. The problem was extended to a helically wrapped ($\beta > 0$) web by Müftü [3]. This work showed that the helical wrap reduces the stiffness of the shell region, leading to higher web-to-guide clearance. The thickness to length ratio of typical webs causes them to be highly susceptible to transverse vibration. Raman et al. [4] investigated the vibrations of isotropic, linearly elastic, stationary and/or translating Kirchoff plates with a low stiffness-to-tension ratio. They showed that the cross-span frequencies of a stationary, uniformly tensioned web, in the absence of fluid loading, clusters around frequencies equivalent to that of a tensioned string. The frequency clustering leads to a dampening in the center of the web span, and positive superposition along the free edges where fluttering is predicted. At low and moderate transport speeds,

* Corresponding author. Tel.: +1 617 373 4743; fax: +1 617 373 2921.
E-mail addresses: s.muftu@neu.edu, smuftu@coe.neu.edu (S. Müftü).

0022-460X/$ - see front matter © 2010 Elsevier Ltd. All rights reserved.
doi:10.1016/j.jsv.2010.08.043

Nomenclature

$a_{\alpha\chi}$	metric tensor
A_i	constant coefficients ($i=1-4$)
$b_{\alpha\chi}$	curvature tensor
$\mathbf{b}$	initial curvature vector
$\mathbf{B}$	matrix of coefficient in the 2D-eigenvalue problem
$\mathbf{B}_b$	bending shape function derivative matrix
$\mathbf{B}_\sigma$	in-plane strain shape function derivative matrix
$\mathbf{B}_s$	transverse shear shape function derivative matrix
C_i	constant coefficients ($i=1-12$)
$\mathbf{c}$	vector of coefficients in the 2D-eigenvalue problem
D_b	bending rigidity, $D_b=Eh^3/12(1-\nu^2)$
D_t	in-plane stiffness $D_t=Eh/(1-\nu^2)$
D_s	shear stiffness $D_s=k_sGc$
$\mathbf{d}$	element degree of freedom (dof) vector
$\ddot{\mathbf{d}}$	acceleration vector of the element dofs
$\mathbf{D}$, $\ddot{\mathbf{D}}$	global dof vector, and its acceleration
$\overline{\mathbf{D}}$	eigenvector
$\mathbf{D}_b$	bending rigidity matrix
$\mathbf{D}_s$	transverse shear rigidity matrix
$e_{\alpha\chi}$	in-plane strains
E	elastic modulus
G	shear modulus
h	web thickness
I	second moment of area
k_s	shear correction factor
k_c	curvature stiffness for beam model
$k(x)$	foundation stiffness of the wrapped beam
$\mathbf{k}^{(e)}$	element stiffness matrix
$\mathbf{k}_b$, $\mathbf{k}_s$	bending and transverse shear element stiffness matrices
$\mathbf{k}_d$, $\mathbf{k}_\sigma$	curvature and tension element stiffness matrices
$\mathbf{K}$	global stiffness matrix
$\mathbf{K}_b$	curvature vector
$\mathbf{K}_s$	transverse shear strain vector
L	total length of the plate
L_1, L_3	lengths of the flat segments of the plate
L_2	length of the wrapped segment of the plate
L_y	plate width
m, n	mode numbers in longitudinal and lateral directions
$M_{\alpha\chi}$	bending moment
$\mathbf{m}^{(e)}$	element inertia (mass) matrix
$\mathbf{M}$	global mass matrix
$N_{\alpha\chi}$	in-plane force resultants
N_i	shape function of a finite element ($i=1-4$)
$\mathbf{N}$	shape function matrix
$\mathbf{N}_d$	shape function matrix
$\mathbf{N}_\phi$	shape function matrix
p	external pressure
Q_α	out-of-plane shear force resultant
r_i, r_i^*	roots of the spatial component of the beam equation ($i=1-4$)
$\mathbf{r}^{(e)}$	element load vector
$\mathbf{r}_\phi$, $\mathbf{r}_\sigma$	element external load and belt-wrap pressure vectors
$R(x, y, \beta)$	radius of the turn-bar expressed in the (x, y) coordinate system
R_c	radius of the cylinder
$S(t)$	temporal component of $w(x, t)$
t	time
T	longitudinal external tension (N/m) plate
T_b	longitudinal external tension (N) beam
$\mathbf{u}$	general dof vector
w	out-of-plane web deflection
$W(x)$	spatial component of the $w(x, t)$
x, y	in-plane coordinates in longitudinal and lateral directions
x_1, x_2	tangency points of the wrapped beam
z	transverse coordinate direction
α, χ	generic plate coordinates in a curvilinear system
β	helix angle
γ_α	shear strain
δ	variational symbol
$\delta_{\alpha\chi}$	Kroenecker delta
$\Delta\lambda$	relative difference in eigenvalues
θ	wrap angle
$\mathbf{\Theta}$	external load vector
$\kappa_{\alpha\chi}$	curvature
λ, λ^-, λ^+,	eigenvalues, anti-symmetric, symmetric
ν	Poisson's ratio of the web
ξ, η	natural coordinates of a quadrilateral element
Π	total potential energy
Π^e	total potential energy of an element
ρ_b	mass per unit length of the beam (kg/m)
ρ_w	mass density of the web (kg/m^3)
$\boldsymbol{\rho}$	element inertia vector
ϕ	shear angle
ψ	shear angle
∇^4	Biharmonic operator

these frequency clusters remain distinct, but merge when translation speed is closer to critical. Ulsoy [5] studied the coupling of spans in vibration of axially moving belts.

The vibration of trapezoidal plates is of interest due to their extensive use in aircraft, space vehicles and ship hulls. No general exact solution has been reported for the free vibration of a trapezoidal plate, which incorporates many complex shapes and different boundary conditions [6], but many approximate solutions for isolated cases are available. The first reported studies of the vibrational characteristics of trapezoidal plates are by Chopra and Durvasula [7,8] in the early 1970s. They applied Galerkin's method, to analyze the free vibration behavior of simply-supported, symmetric and unsymmetric plates by expressing the deflection with Fourier sine series in transformed coordinates. Fundamental

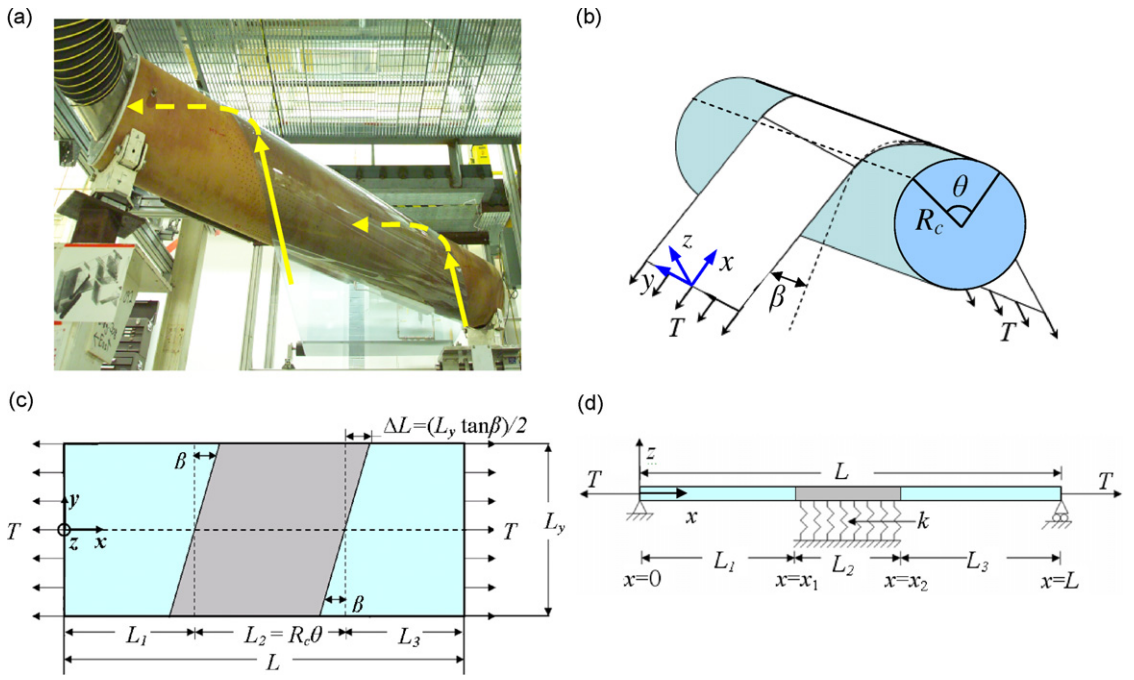

Fig. 1. (a) A typical polymer-based web wrapped helically around a turn-bar (courtesy of Dr. Kevin Cole, Optimation Technology Inc., Rush, NY 14543). (b) Schematic representation of the turn-bar application. (c) Geometry of tensioned web under study. The gray area highlights the shell area surrounded by flat (plate) sections. The two edges in the longitudinal direction, at $x=0,L$ are simply supported, and lateral edges are free. (d) Geometry of the wrapped-beam model.

frequencies and respective mode shapes were given for plates with different geometries. This method, however, is only applicable to simply supported trapezoidal plates due to the chosen functions describing the plate. Qatu et al. [9] presented a solution for the natural frequencies of trapezoidal plates with free boundaries. The Rayleigh–Ritz method was applied with appropriate algebraic polynomials satisfying the boundary conditions. Liew and Lam [10] utilized orthogonal shape functions in conjunction with Rayleigh–Ritz method to solve a combination of clamped, simply-supported and free-edge support conditions for isotropic and anisotropic trapezoidal plates. The Rayleigh–Ritz method is powerful to solve this problem, but limited by the need for geometry specific functions.

The present work investigates the transverse vibration characteristics of a thin, tensioned plate wrapped helically around a cylinder (e.g. turn-bar) (Fig. 1). It is assumed that the air cushion provided by the turn-bar provides a gap in the shell area, but the fluid–structure coupling is not included in this work. Moreover, the web transport is assumed to take place at low speeds. Therefore, the gyroscopic effects due to web transport, analyzed extensively in references [11–13], are excluded from this study. In this work, a customized finite element program was developed to study the eigenvalue problem. This approach provides modeling flexibility, and avoids the need to find customized mode-shape functions to handle the boundary and continuity conditions between the flat and wrapped segments of the system.

2. Governing equation

First, the partial differential equation (PDE) governing the equilibrium of a plate wrapped around a cylindrical drum (turn-bar), as shown in Fig. 1, is derived by using the energy method. Wrapping an initially flat plate around a cylinder causes bending moments to be "stored" in the wrapped segment of the plate, and thus modifies the out-of-plane deflection behavior. Mechanics of a helically wrapped plate around a cylindrical drum has been treated by Rongen [14,15]. His work is based on the Donnell–Mushtari–Vlasov (DMV) cylindrical shell theory [16,17], which is an extension of von Karman's plate theory. Rongen formulated the problem by the energy method and developed a finite element solution. Müftü obtained a set of partial differential equations for the same system by using the equilibrium method within the context of the DMV theory, and demonstrated the effect of the helical wrap on the shell stiffness of the system [3]. In the present work, the equation of equilibrium in the out-of-plane direction and the corresponding boundary conditions are derived by using the energy method. The following, Kirchhoff–Love, assumptions are used in this derivation: (i) the normals of deformed and undeformed middle surface are assumed to remain straight with no extension; (ii) the transverse normal stress is assumed to be negligible when compared to the other components of stress; and (iii) the displacements of the shell are assumed to be small compared to the thickness.

Mechanics of the wrapped plate is modeled with respect to the (x, y) coordinate system located in its middle plane. Fig. 1c shows an unwrapped depiction of the middle plane, where x-, y- and z-axis are oriented along the longitudinal, lateral and transverse directions of the web. This depiction reveals that the helically wrapped web is composed of two trapezoidal flat plate segments that are joined to a trapezoidal cylindrical shell segment of radius R_c. The wrap angle, θ, represents the direction change that the web undergoes in the circumferential direction of the turn-bar, and the helix angle, β, represents how much the web climbs along the axial direction of the turn-bar, in a barber-pole fashion. Note that the web's radius of curvature would be expected to transition from its value in the wrap region to infinity in the plate region in a finite distance. However, the length of this transition region has been shown to be small with respect to the overall dimensions of the web [2] and it is neglected in this work.

The plate material is assumed to behave in a linearly elastic manner. The constitutive equations of an isotropic shell are given as follows [16]:

$$N_{\alpha\chi} = D_t[(1-\nu)e_{\alpha\chi} + \nu a_{\alpha\chi} e_{\gamma\gamma}] \tag{1a}$$

$$M_{\alpha\chi} = -D_b[(1-\nu)\kappa_{\alpha\chi} + \nu a_{\alpha\chi}\kappa_{\gamma\gamma}] \tag{1b}$$

$$Q_\alpha = D_s\gamma_\alpha \tag{1c}$$

where $D_b = Eh^3/12(1-\nu^2)$ is the bending rigidity, $D_t = Eh/(1-\nu^2)$ is the in-plane stiffness, $D_s = k_sGh$ is the shear stiffness, E is the elastic modulus, G is the shear modulus, k_s is the shear correction factor, ν is the Poisson's ratio, and h is the thickness of the shell. Note that the subscripts α and χ represent the in-plane directions and take the values (x, y) for longitudinal and lateral directions, respectively as shown in Fig. 1. $a_{\alpha\chi}$ is the metric tensor. The membrane strain, $e_{\alpha\chi}$, transverse shear strain, γ_α, and curvature, $\kappa_{\alpha\chi}$, are defined as follows:

$$e_{\alpha\chi} = u_{\alpha,\chi} - b_{\alpha\chi}w + \tfrac{1}{2}w_{,\alpha}w_{,\chi} \tag{2a}$$

$$\gamma_\alpha = w_{,\alpha} \tag{2b}$$

$$\kappa_{\alpha\chi} = w_{,\alpha\chi} + b_{\alpha\chi} \tag{2c}$$

where u_α and w represent the in-plane and the out-of-plane displacement components, respectively, $b_{\alpha\chi}$ is the curvature tensor, and a subscripted comma indicates a partial derivative.

Note that the curvature tensor, $b_{\alpha\chi}$, represents the normal curvature of the middle surface of the shell, and thus provides a means to include the effect of the "stored" bending moments applied to bend the web around the turn-bar in a helical fashion [2,3,15]. It was shown in reference [3] that $b_{\alpha\chi}$ can be given as follows:

$$b_{xx} = -\frac{\cos^2\beta}{R}, \quad b_{yy} = -\frac{\sin^2\beta}{R}, \quad b_{xy} = b_{yx} = \frac{\sin\beta\cos\beta}{R} \tag{3}$$

where R is the radius of the turn-bar, which is defined with respect to the (x, y) coordinate system of the web as follows:

$$\frac{1}{R(x,y,\beta)} = \begin{cases} 0 & \text{for} \quad -\dfrac{L_y}{2} \le y \le \dfrac{L_y}{2} \quad \text{and} \quad 0 \le x \le (L_1 + y\tan\beta) \\ R_c^{-1} & \text{for} \quad -\dfrac{L_y}{2} \le y \le \dfrac{L_y}{2} \quad \text{and} \quad (L_1 + y\tan\beta) < x < (L_1 + L_2 + y\tan\beta) \\ 0 & \text{for} \quad -\dfrac{L_y}{2} \le y \le \dfrac{L_y}{2} \quad \text{and} \quad (L_1 + L_2 + y\tan\beta) \le x \le L \end{cases} \tag{4}$$

The metric tensor $a_{\alpha\chi}$ relates the change in arc length on a curved surface to the change in curvilinear coordinate, and when an orthogonal coordinate system such as the one shown in Fig. 1c is used it can be shown that [3]

$$a_{\alpha\chi} = \delta_{\alpha\chi} \tag{5}$$

where $\delta_{\alpha\chi}$ is the Kroenecker delta.

The governing equation and the essential and natural boundary conditions of the problem are found by using the energy formulation. The total potential energy of the system is given as follows:

$$\Pi = \frac{1}{2}\int_A (M_{xx}\kappa_{xx} + 2M_{xy}\kappa_{xy} + M_{yy}\kappa_{yy})\,dA + \int_A \left(\frac{1}{2}N_{xx} + T\right)\varepsilon_{xx}\,dA - \int_A pw\,dA \tag{6}$$

where M_{xx} and M_{yy} are the bending moments and M_{xy} is the twisting moment, defined in Eq. (1b), the terms κ_{xx}, κ_{yy} and κ_{xy} are the corresponding curvature terms, defined in Eqs. (2c), T is the initial longitudinal tension in the web, N_{xx} is the in-plane membrane stress resultant, defined in Eq. (1a) and p is the external pressure. The strain energy stored in bending and stretching during deformation are represented by the first two terms of this equation, whereas the last term represents the work done by the external pressure.

In this work, the effects of the in-plane displacements u_x and u_y, and the membrane stress resultants N_{yy} and N_{xy} are neglected. However, the effects of the longitudinal in-plane stress resultant N_{xx} due to out-of-plane deflection, w, of the web are included. The total potential energy of the system is then expanded and written in terms of displacement, w, and

initial curvature, $b_{\alpha\chi}$, by using Eqs. (1)–(5) as follows:

$$\Pi = \frac{1}{2}D_b\int_A[((w_{,xx}+b_{xx})+(w_{,yy}+b_{yy}))^2-2(1-\nu)((w_{,xx}+b_{xx})(w_{,yy}+b_{yy})-(w_{,xy}+b_{xy})^2)]\,dA + \int_A\left[\frac{1}{2}D_t(b_{xx}^2+\nu b_{xx}b_{yy})w^2+T\left(-b_{xx}w+\frac{1}{2}w_{,x}^2\right)\right]dA+\int_A pw\,dA \tag{7}$$

Note that this expression is obtained by excluding the terms that would lead to nonlinearity in w. The principle of minimum total potential energy requires the variation of the total potential energy to be $\delta\Pi=0$ at steady state equilibrium, which gives:

$$\delta\Pi = D_b\int_A[(w_{,xx}+b_{xx})\delta w_{,xx}+\nu((w_{,xx}+b_{xx})\delta w_{,yy}+(w_{,yy}+b_{yy})\delta w_{,xx})]\,dA + D_b\int_A[(w_{,yy}+b_{yy})\delta w_{,yy}+2(1-\nu)(w_{,xy}+b_{xy})\delta w_{,xy}]\,dA+D_t\int_A[(b_{xx}^2+\nu b_{xx}b_{yy})w\delta w]\,dA + T\int_A[-b_{xx}\delta w+w_{,x}\delta w_{,x}]\,dA-\int_A p\delta w\,dA=0 \tag{8}$$

Upon integration by parts, collecting the terms, and using the definition of the curvature components given in Eq. (3), the equilibrium equation is found as follows:

$$D_b\nabla^4 w+\frac{D_t\cos^2\beta(\cos^2\beta+\nu\sin^2\beta)}{R^2(x,y,\beta)}w-Tw_{,xx}=p-\frac{T}{R(x,y,\beta)}\cos^2\beta \tag{9}$$

This equation is identical to that derived from the local equilibrium considerations in Ref. [3]. The integration by parts of Eq. (8) shows that along the longitudinal edges, $x=0$, L and $-L_y/2\le y\le -L_y/2$, the following boundary conditions can be prescribed:

$$D_b[(w_{,xx}+b_{xx})+\nu(w_{,yy}+b_{yy})]=0 \quad \text{or} \quad w_{,x}\ \text{prescribed} \tag{10}$$

and

$$D_b[w_{,xxx}+(2-\nu)w_{,xyy}]-Tw_{,x}=0 \quad \text{or} \quad w\ \text{prescribed} \tag{11}$$

Similarly along the lateral edges, $y=-L_y/2$, $L_y/2$ and $0\le x\le L$, the following boundary conditions are possible:

$$D_b[(w_{,yy}+b_{yy})+\nu(w_{,xx}+b_{xx})]=0 \quad \text{or} \quad w_{,y}\ \text{prescribed} \tag{12}$$

and

$$D_b[w_{,yyy}+(2-\nu)w_{,yxx}]=0 \quad \text{or} \quad w\ \text{prescribed} \tag{13}$$

Finally, on the corners $x=0$, L and $y=-L_y/2$, $L_y/2$, the following corner conditions are found:

$$2D_b(1-\nu)(w_{,xy}+b_{xy})=0 \quad \text{or} \quad w\ \text{prescribed} \tag{14}$$

Eqs. (10) and (12) show that along the boundary either the bending moments must be zero, or the slopes must be prescribed. Similarly, Eqs. (11) and (13) show that either the shear force resultant must be zero or the displacement must be prescribed. The first terms given in Eqs. (10)–(13) are the natural boundary conditions, and the second terms are the essential boundary conditions; only one of the two conditions must be satisfied along a given boundary. Notice in the moment boundary conditions, the initial curvature terms $b_{\alpha\chi}$ defining the helical shell are included. Also notice, that the boundary condition on the shear force resultant in Eq. (11) contains an added term accounting for the in-plane stiffening due to external tension T.

3. Effect of curvature

In order to investigate the effect of the wrapped region on the vibration response of the web, it is instructive to study a beam model that is partially supported by an elastic foundation, as shown in Fig. 1d. The beam model is representative of the mid-section of the plate ($y=0$, $0\le x\le L$) with $\beta=0$. The equation of motion of such a beam is obtained from Eq. (9) as follows:

$$\rho_b\ddot{w}+EIw_{,xxxx}-T_bw_{,xx}+k(x)w=0 \tag{15}$$

where the stiffness of the elastic foundation is

$$k(x)=\begin{cases}0 & \text{for} \quad 0\le x<x_1\\ \dfrac{EhL_y}{R_c^2} & \text{for} \quad x_1\le x\le x_2\\ 0 & \text{for} \quad x_2<x\le L\end{cases} \tag{16}$$

where E is the elastic modulus, I is the second moment of area, L_y is the width, T_b is the tension, ρ_b is the mass per unit length and w is the transverse deflection of the beam. Note that the inertial force $\rho_b\ddot{w}$ is included by using D'Alembert's principle, but the effect of possible damping is neglected in this work. The superscripted "." indicates the time derivative. In general, the method of separation of variables can be used to represent the deflection as $w(x,t)=W(x)S(t)$. Substituting into Eq. (15), we find the following general relationship:

$$S(t)=e^{\lambda t} \quad \text{and} \quad W(x)=A_1e^{r_1x}+A_2e^{r_2x}+A_3e^{r_3x}+A_4e^{r_4x} \tag{17}$$

with

$$r_{1,2,3,4}=\pm\frac{1}{\sqrt{2}}\sqrt{\frac{T_b}{EI}\pm\sqrt{\left(\frac{T_b}{EI}\right)^2+4\frac{\rho_b\lambda^2-k}{EI}}}$$

where λ represents the eigenvalues (natural frequencies) of the system, A_i are constant coefficients, and $k=k(x)$ as defined in Eq. (16). Due to the discontinuous nature of this curvature stiffness, the system behavior is sought for the three segments of the beam separately and leads to the following relationship:

$$W(x)=\begin{cases} C_1\sinh(r_1^*x)+C_2\cosh(r_2^*x)+C_3\sin(r_3^*x)+C_4\cos(r_4^*x) & \text{for} \quad 0\le x<x_1 \\ C_5e^{r_1x}+C_6e^{r_2x}+C_7e^{r_3x}+C_8e^{r_4x} & \text{for} \quad x_1\le x\le x_2 \\ C_9\sinh(r_1^*x)+C_{10}\cosh(r_2^*x)+C_{11}\sin(r_3^*x)+C_{12}\cos(r_4^*x) & \text{for} \quad x_2<x\le L \end{cases} \tag{18}$$

Note that for straight segments of the beam $k=0$, and the roots r_1–r_4 from Eq. (17) are adjusted accordingly. This is denoted by the superscript "*". To solve for the twelve constant coefficients, C_1-C_{12}, the boundary and continuity conditions are employed. Four conditions come from the simple-support boundary conditions at the ends $x=0$ and L, and the other eight conditions come from the continuity requirement of the deflection, the slope, the internal moment and the internal shear force at $x=x_1$ and x_2. Implementing these conditions on Eq. (18), a set of twelve homogeneous algebraic equations is developed. This system is represented in matrix form as follows:

$$\mathbf{B}\cdot\mathbf{c}=0 \tag{19}$$

where $\mathbf{c}$ contains the vector of unknown coefficients from Eq. (18). A non-trivial solution of Eq. (19) is only possible when

$$\det\mathbf{B}=0 \tag{20}$$

For given set of problem parameters (i.e. E, L_y, h, T_b, etc.) the determinant is solely a function of the eigenvalues, λ. Eq. (20) represents the characteristic equation of the system for infinitely many eigenvalues. The solution of this equation is obtained by using Mathematica (ver. 5.0 Champaign, IL). For a given eigenvalue λ the corresponding eigenvector (mode shape) is found from (19) by solving for the coefficients in terms of one specified coefficient.

3.1. Effect of wrapping analyzed

Dynamic response of a tensioned beam wrapped around a cylindrical guide is analyzed in Figs. 2–4 for different thickness, tension, guide radius and beam lengths. The predominant effect observed is that the wrapped segment of the beam can isolate or contribute into the vibration response of the flat segments depending on the problem parameters. Fig. 2 shows that a beam that has flat segments with equal lengths ($L_1=L_3$), has *symmetric* and *anti-symmetric* vibration mode shapes, that are designated with the "+" and "−" symbols, respectively. The excitation of the flat and curved beam segments remains largely independent, due to the added curvature (shell) stiffness in the wrapped region. This condition creates an effective support at the boundary of the flat and curved segments, resisting the transverse motion. The order of appearance of the symmetric/anti-symmetric modes, and the magnitude of their frequencies depend on the effectiveness of this boundary to act as a support, which in turn depends on the bending rigidity EI, curvature stiffness, $k_c=EhL_y/R_c^2$, the span lengths, L_1, L_2 and L_3, and the tension, T_b. For the typical web thickness values of $h=5-250$ μm, the response of the wrapped region has been found to be minimal. Therefore, a relatively thick beam of $h=1$ cm is used, only in Figs. 2 and 3 in order to visually demonstrate the effects of vibrations on the wrap region. Note that in these two examples the thickness to span ratio is always smaller than 0.05, which is within the range of validity of the Euler–Bernoulli beam theory.

In order to better illustrate the function of the boundary between the flat and the curved segments, the curved region's modal response is presented for different lengths ($L_2=1$ and 0.5 m). In Fig. 3a, where $L_2=1$ m, only a small length of the wrapped segment deforms, regardless of mode symmetry. But, as the length of the curved region decreases, as shown in Fig. 3b, where $L_2=0.5$ m, the flat-to-curved boundary allows more deformation. It is thus seen that a longer wrapped region is more effective to serve as a stiff boundary for these parameters. It should be noted that anti-symmetric modes appear before symmetric modes (i.e. $\lambda^{(-)}<\lambda^{(+)}$) as they require less energy for excitation.

In modeling the mechanics of a web in the free span between two guides, simple-support conditions are commonly used to model the guides (e.g. [1]). Next, a comparison is made between the natural frequencies of a wrapped beam and a simply-supported beam with length $L=L_1=L_3$ in Fig. 4. Note that the inset in this figure depicts the compared boundary conditions, and the beam thickness is $h=100$ μm for this analysis. The curvature stiffness, $k_c=EhL_y/R_c^2$, is varied by changing the wrap radius, but holding $L_2=0.5$ m. The results are reported by using the relative difference in eigenvalues

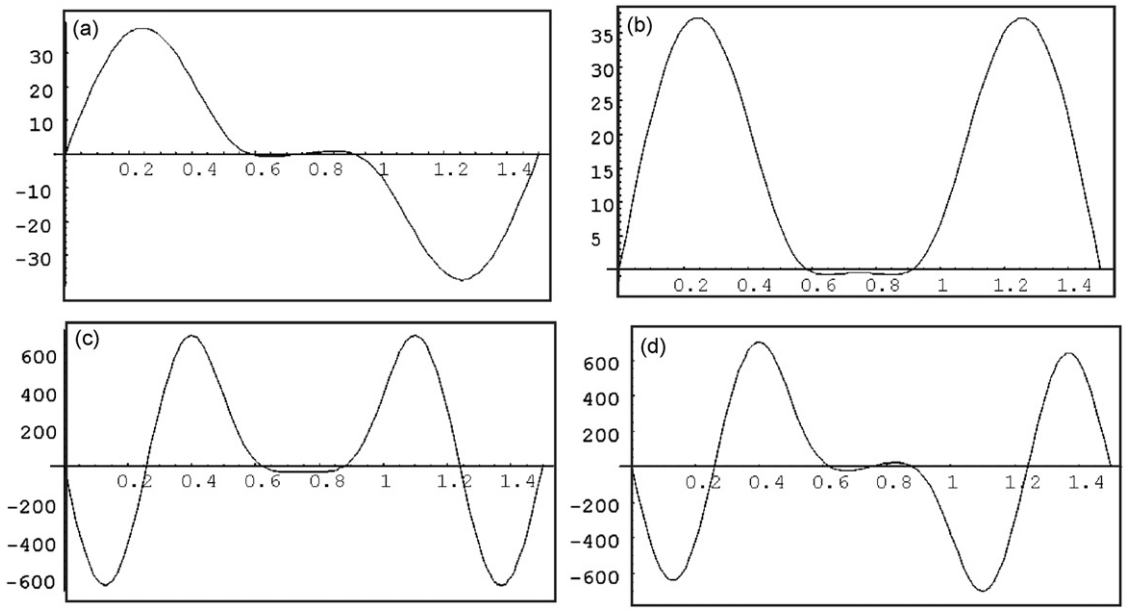

Fig. 2. First four beam eigenmodes for $L_1=L_2=L_3=0.5$ m, $L_y=0.01$ m, $h=0.01$ m, $R_c=1$ m and $T_b=150$ N. (a) Beam mode, $m=-1$ and $\lambda^{(-)}=238.37$ rad/s; (b) beam mode, $m=+1$ and $\lambda^{(+)}=238.48$ rad/s; (c) beam mode, $m=+2$ and $\lambda^{(+)}=748.7$ rad/s; (d) beam mode, $m=-2$ and $\lambda^{(-)}=749.26$ rad/s.

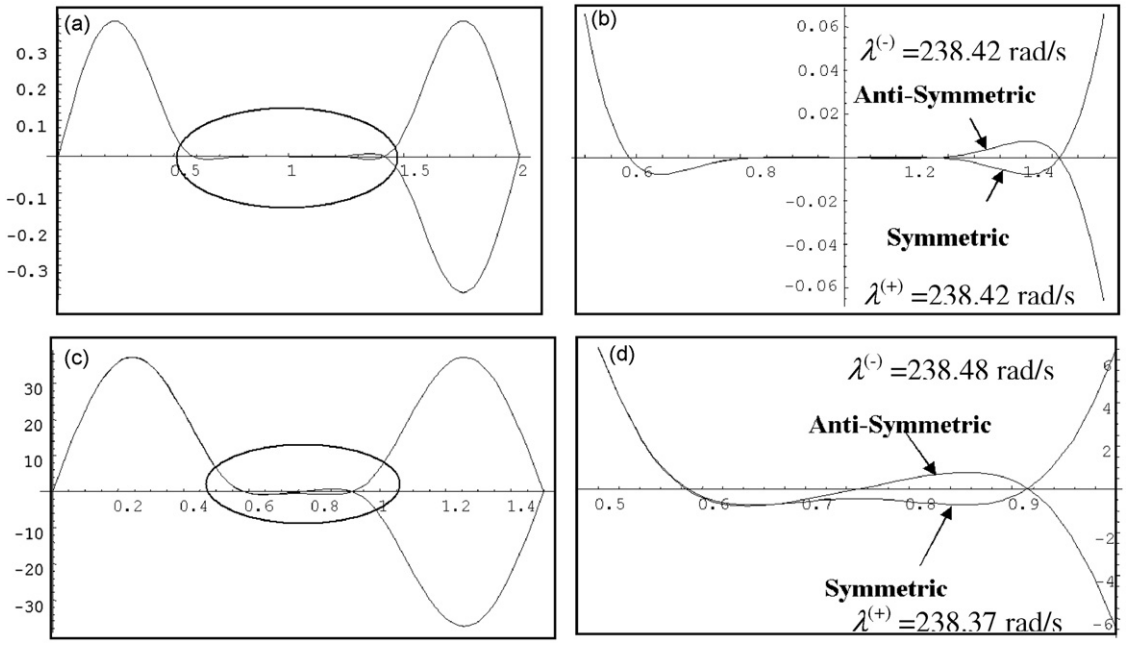

Fig. 3. Comparison of shell responses with varying stiffness for symmetric (+) and anti-symmetric (−) modes for beam model. Shell length is changed to vary stiffness. Beam parameters are as follows: $L_1=L_2=L_3=0.5$ m, $L_y=0.01$ m, $h=0.01$ m, $R_c=1$ m and $T_b=150$ N. (a) $L_2=1.0$ m, (b) detail of the wrapped region given in (a), (c) $L_2=0.5$ m and (d) detail of the wrapped region given in (c).

$\Delta\lambda=(\lambda_{\text{Wrapped-beam}}-\lambda_{\text{SS-beam}})/\lambda_{\text{SS-beam}}$ as a function of guide radius and tension. The differences in the first eigenvalues are shown in Fig. 4a, b for $L_1=L_3=1$ and 0.2 m, respectively. It is seen that for small guide radii, the eigenvalues of the wrapped-beam system are higher than the simply supported beam, shown on the inset. This indicates that in this case the wrapped segment of the beam represents a support condition that is stiffer than the simple support. Such stiffness is attributed to the non-zero moment reaction at the wrapped end.

However, the situation is even more involved as the transverse vibration could also change the distance between the presumed supports locations. In fact, such a situation is encountered in this example. Increasing the guide radius, thus

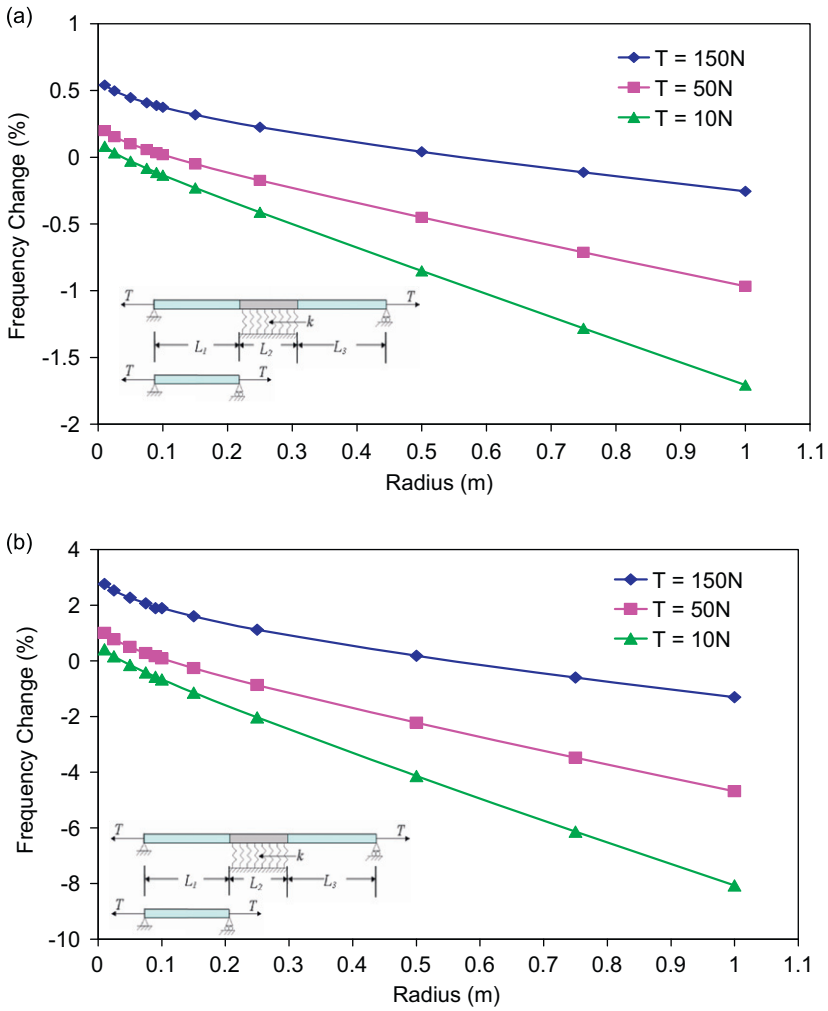

Fig. 4. The effect of the length of the flat beam segments (L_1, L_3) on the relative difference $\Delta\lambda$ of the first natural frequencies as a function of wrap radius and tension. Plotted for T_b=10, 50 and 150 N, L_y=0.5 m, L_2=0.5 m and h=100 μm. An example of the beams used in the comparison is superimposed on the charts. (a) L_1=L_3=1 m and (b) L_1=L_3=0.2 m.

weakening the curvature stiffness, leads to eigenvalues that are lower than those of the beam with the idealized simple-support conditions. For the larger radii, larger spans of the beam are being excited. The extreme case would be a zero curvature, stiffness and full excitation of the entire length of the wrapped beam. These effects are more pronounced for lower tension values. Comparison of Fig. 4a, b also shows that the difference in natural frequencies predicted by the wrapped-beam model, and the simply-supported beam model grows as the length of the straight beam segment is reduced. This analysis gives guidance to the accuracy of modeling the beam mechanics over a wrap region by using simple-support boundary condition.

4. Eigenvalue analysis of the helically wrapped plates

Early work on the FE solution of plates and shells was based on Kirchhoff's hypothesis which neglects the effects of shear deformation by assuming planes normal to the mid-surface remain normal after deformation. These solutions are limited to thin plates since rotations are found directly from displacements; shape functions require at least C^1 continuity. This led to numerous difficulties in developing higher-order plate elements needed to model abnormal geometries. Although advancements have been made using Kirchhoff based elements [18] many recent FE models, and the one used in this analysis, are based upon the Mindlin theory of plate bending.

Mindlin plate theory accounts for transverse shear deformation with the assumption that planes normal to the mid-surface need not remain normal after the loads are applied. In this theory, the rotation variables are decoupled from the normal displacement, w, which allows for elements of C^0 continuity. The use of lower-order elements reduces the complexity of the formulation, and inclusion of shear strain extends the method's ability to model relatively thick plates

and shells. There is, however, a significant drawback to using C^0 elements when the span-to-thickness ratio becomes very large. As the element becomes thinner the solution predicts spurious shear stresses causing an under-prediction of displacements known as *shear locking*.

Shear locking results from the inability of shear deformable elements to properly model the curvatures within an element under a state of zero transverse shearing strain (i.e. pure bending). It was discovered in the late 1970s by both Zienkiewicz [19,20] and Hughes [21,22] that an adequate bending element can be obtained with the use of selective or reduced integration. In the 1980s, mixed interpolation and degenerative element theories were proposed by Lee and Wong [23] and Bathe and Dvorkin [24]. Donea and Lamain [25] used modified shear polynomials for four-, eight- and nine-node quadrilateral elements. Pinsky and Jasti [26] made use of bubble functions to alleviate shear locking with mixed FE formulation. In the early 1990s, advances were made on various quadrilateral elements using assumed strain fields and mixed interpolation theories by Shi and Voyiadjis [27], Kim and Choi [28], Bucalem and Bathe [29], Bathe [30], and Politet al. [31]. Bletzinger et al. [32] used the "discrete shear gap" method to alleviate locking which is shown to produce quite accurate results for linear problems. Successful triangular elements have been created by Marczak and Awruch [33] for shells and by Kabir [34] for thick and thin plates. Ultimately, the most efficient procedure to be used will depend on the type of model being created. In this work, the procedure outlined by Donea and Lamain [25] for a four-node quadrilateral element is used to alleviate shear locking [35,36].

The total potential energy of the system, including the effects of transverse shear, is given as follows:

$$\Pi = \frac{1}{2}\int_A \mathbf{K}_b^{\mathrm{T}}\mathbf{D}_b\mathbf{K}_b\,dA + \int_A\left(\frac{1}{2}N_x + T\right)\varepsilon_x\,dA + \frac{1}{2}\int_A \mathbf{K}_s^{\mathrm{T}}\mathbf{D}_s\mathbf{K}_s\,dA - \int_A pw\,dA \tag{21}$$

where $\mathbf{K}_b$ and $\mathbf{K}_s$ are curvature and shear deflection vectors, respectively, defined as follows:

$$\mathbf{K}_b = \begin{Bmatrix} \psi_{,x} + b_{xx} \\ \phi_{,y} + b_{yy} \\ \psi_{,y} + \phi_{,x} + 2b_{xy} \end{Bmatrix} \quad \text{and} \quad \mathbf{K}_s = \begin{Bmatrix} w_{,x} + \psi \\ w_{,y} + \phi \end{Bmatrix} \tag{22}$$

where ψ and ϕ are the angles of rotation of the normal to the middle surface, in the x–z-plane and y–z-plane, respectively. The bending rigidity matrix, $\mathbf{D}_b$ and the shear rigidity matrix, $\mathbf{D}_s$, for an isotropic plate/shell are given as follows:

$$\mathbf{D}_b = \frac{h^3}{12(1-\nu^2)}\begin{bmatrix} E & \nu E & 0 \\ \nu E & E & 0 \\ 0 & 0 & G(1-\nu^2) \end{bmatrix} \quad \text{and} \quad \mathbf{D}_s = k_s G h \begin{bmatrix} 1 & 0 \\ 0 & 1 \end{bmatrix} \tag{23}$$

Eq. (21) differs from (7) only by inclusion of the transverse shear terms.

Bilinear, quadrilateral Mindlin elements are used for discretization of the plate. The degrees of freedom, $\mathbf{u}$, are interpolated over an element using shape functions, $\mathbf{N}$, and the nodal degrees of freedom, $\mathbf{d}$ as follows:

$$\mathbf{u} = \begin{Bmatrix} \psi \\ \phi \\ w \end{Bmatrix} = \mathbf{N}\bullet\mathbf{d} \tag{24}$$

where the shape function matrix N and the degree of freedom vector d are given as follows:

$$\mathbf{N} = \begin{bmatrix} N_i & 0 & 0 \\ 0 & N_i & 0 \\ 0 & 0 & N_i \end{bmatrix} \quad \text{and} \quad \mathbf{d} = \begin{Bmatrix} \psi_i \\ \phi_i \\ w_i \end{Bmatrix}_{12\times 1} \tag{25}$$

where the subscript, i, denotes the node number of the element, with i=1, …, 4. Each node of the element has an initial curvature, denoted in the curvature vector as follows:

$$\mathbf{b} = \begin{Bmatrix} b_{xx_i} \\ b_{yy_i} \\ 2b_{xy_i} \end{Bmatrix}_{12\times 1} \tag{26}$$

The total potential energy for a single element is expressed as follows:

$$\begin{aligned} \Pi^e = {} & \frac{1}{2}\int_A (\mathbf{b}^{\mathrm{T}} + \mathbf{d}^{\mathrm{T}}\mathbf{B}_b^{\mathrm{T}})\mathbf{D}_b(\mathbf{B}_b\mathbf{d} + \mathbf{b})\,dA + \frac{1}{2}D_t\int_A (b_{xx}^2 + \nu b_{xx}b_{yy})\mathbf{d}^{\mathrm{T}}\mathbf{N}_d^{\mathrm{T}}\mathbf{N}_d\mathbf{d}\,dA \\ & + T\int_A\left(b_{xx}\mathbf{d}^{\mathrm{T}}\mathbf{N}_d^{\mathrm{T}} + \frac{1}{2}\mathbf{d}^{\mathrm{T}}\mathbf{B}_\sigma^{\mathrm{T}}\mathbf{B}_\sigma\mathbf{d}\right)dA + \frac{1}{2}\int_A \mathbf{d}^{\mathrm{T}}\mathbf{B}'^{\mathrm{T}}_s\mathbf{D}_b\mathbf{B}'_s\mathbf{d}\,dA - \int_A \mathbf{d}^{\mathrm{T}}\mathbf{N}_d^{\mathrm{T}}\mathbf{N}_\Phi\boldsymbol{\Theta}\,dA \end{aligned} \tag{27}$$

where $\mathbf{B}_b$, $\mathbf{B}_\sigma$ and $\mathbf{B}'_s$ are the shape function derivative matrices $\mathbf{N}_d$ and $\mathbf{N}_\Phi$ are shape function matrices, and $\boldsymbol{\Theta}$ is the nodal load vector, all of which are defined in Appendix A. The total potential energy is minimized with respect to the nodal degrees of freedom vector, $\mathbf{d}$, resulting in the element equilibrium equations:

$$\mathbf{k}^{(e)}\mathbf{d} = \mathbf{r}^{(e)} \quad \text{with}$$

Table 1
Parameters used in this study reflect typical parameters for a web handling application.

R_c (m)	0.15
θ (deg.)	30, 180
L_1 (m)	0.2, 1
L_3 (m)	0.2, 1
L_y (m)	0.25, 0.5
h (μm)	100
T (N/m)	5, 10, 50, 150
β (deg.)	0, 5, 10, 22.5, 45
E (GPa)	4.5

$$\mathbf{k}^{(e)} = (\mathbf{k}_b + \mathbf{k}_s + \mathbf{k}_d + \mathbf{k}_\sigma)$$
$$\mathbf{r}^{(e)} = \mathbf{r}_\Phi - \mathbf{r}_\sigma \tag{28}$$

where $\mathbf{k}_b$,$\mathbf{k}_s$,$\mathbf{k}_d$ and $\mathbf{k}_\sigma$ represent the bending, transverse shear, curvature and tension components of the element stiffness, and $\mathbf{r}_\Phi$ and $\mathbf{r}_\sigma$ represent the external load and the belt-wrap pressure acting on the element nodes, respectively.

As before, the equation of motion for a single element is obtained by using D'Alembert's principle as follows:

$$\mathbf{m}^{(e)}\ddot{\mathbf{d}} + \mathbf{k}^{(e)}\mathbf{d} = \mathbf{r}^{(e)} \tag{29}$$

where the consistent mass matrix $\mathbf{m}^{(e)}$ for the same bilinear, quadrilateral, Mindlin element is given as follows:

$$\mathbf{m}^{(e)} = \int \boldsymbol{\rho}\mathbf{N}^{\mathrm{T}}\mathbf{N}\,dA \tag{30}$$

with

$$\boldsymbol{\rho}_i^{\mathrm{T}} = \left\{ \rho_{w_i} \quad \frac{1}{12}\rho_w h_i^2 \quad \frac{1}{12}\rho_w h_i^2 \right\}$$

The global equation of motion is obtained from force balance at each node, resulting in the following relationship:

$$\mathbf{M}\ddot{\mathbf{D}} + \mathbf{K}\mathbf{D} = \mathbf{R} \tag{31}$$

where $\mathbf{D}$ is the global nodal degrees of freedom vector, $\ddot{\mathbf{D}}$ is the corresponding acceleration vector, and $\mathbf{M}$ and $\mathbf{K}$ are the global mass and stiffness matrices. The displacement w along the longitudinal edges, x=0, L, are fixed.

The eigenvalues of the system can be found by assuming that modes move synchronously as $\mathbf{D}(x,y,t)=\overline{\mathbf{D}}e^{\lambda t}$. Using the stiffness and mass matrices outlined above, we can define an eigenvalue problem to perform an undamped, free vibration analysis of a plate wrapped around the cylinder. This problem is defined as follows:

$$(\mathbf{K}-\lambda^2\mathbf{M})\overline{\mathbf{D}} = 0 \tag{32}$$

where λ's are the eigenvalues and $\overline{\mathbf{D}}$ are the associated eigenvectors (mode shapes). The symmetric, banded Lapack eigenvalue/vector solution routine DSBGV was used to solve the eigenvalue problem [37].

In order to examine the effect of the mesh size on the predicted eigenvalues, a convergence study was conducted. The free vibration response of a tensioned, cylindrically wrapped tape by Sundaram and Benson [38] was used to verify the eigenvalues and eigenvectors for both plate and shell solutions. A mesh convergence study was conducted for tensioned plate and cylindrical shell configurations separately. These structures were simply-supported along the longitudinal edges and free along the lateral edges. The dimensions of the plates and shells were on the same order of the cases studied during the design parameter analysis of the coupled system (Table 1).

As expected, this study showed that the lateral vibration modes are excited more easily than the longitudinal modes, and this is attributed to the presence of free lateral edges. Through numerical experiments it was found that, to have a robust model for all the anticipated longitudinal and helical wrap configurations, a mesh of at least 21 nodes in the longitudinal direction and 121 nodes in the lateral direction is necessary for each plate/shell section of the coupled system. With this mesh size, the maximum error per uncoupled plate/shell was shown to be less than 1.4% [39]. The coupled plate-shell-plate system mesh consists of three sections, for a total of 61 nodes in the longitudinal and 121 nodes in the lateral directions. The size of the elements then become $\Delta x_1=L_1/20$, $\Delta x_2=L_2/20$, $\Delta x_3=L_3/20$ in the longitudinal direction and $\Delta y=L_y/120$ in the lateral direction. The lengths L_1, L_2 and L_3 were chosen in the range of 0.2–1 m, and the width L_y was chosen in the range 0.2–0.5 m. In order to check the convergence of the results for the helically wrapped case, a trapezoidal plate, i.e. the flat segment of a helically wrapped plate, was modeled with the commercially available finite element software package ANSYS [39] using a similar meshing scheme. No significant differences were seen between the dominant eigenvalues of the helically wrapped case and the ANSYS results.

5. Results and discussion

The numerical analysis of the eigenvalue problem outlined in Section 4 shows that the mode shapes can be identified by their *longitudinal* and *lateral* components indicated by m and n, respectively. This is especially applicable for the zero helix angle (i.e., $\beta=0$) case, as expected. For helically wrapped webs, the mode-shape descriptions are similar, as will be introduced shortly. First, the mode shapes and eigenvalues for $\beta=0$ case are introduced, and compared to the wrapped-beam model. The base parameters are chosen from a typical web handling case, and they are given in Table 1.

As in the case of the wrapped beam, a wrapped plate with equally long flat segments ($L_1=L_3$) has eigenmodes which have the same mode numbers, but are symmetric or anti-symmetric about the center of the plate. Fig. 5 shows examples of modes $m=1$ and $n=\pm0,\ \pm1,\ \pm2$. The natural frequencies for the eigenmodes $m=1$ and $n=0$ can be predicted by the beam model. In Fig. 6a, b the eigenvalues for modes $m=1$ and $n=\pm0,\ \pm1,\ \ldots,\ \pm6,\ -7$ are shown for two wrap angles, $\theta=30^\circ$ and 180°, and two different wrapped plates, with $L_1=L_3=1$ and 0.2 m, respectively. In these figures, the eigenvalues of the symmetric and anti-symmetric lateral (n) modes are plotted separately. In the case with the longer flat segments, given in Fig. 6a, all of the modes nearly coincide for different wrap angle, θ, values. On the other hand, in the case with shorter flat segments, presented in Fig. 6b, the natural frequencies are distinctly different for the symmetric/anti-symmetric modes, and for different wrap angles. The effect is magnified for the smaller wrap angle, which was shown to represent a weaker support condition for the plate/shell boundary. The frequency magnitude also decreases for the first 15 modes.

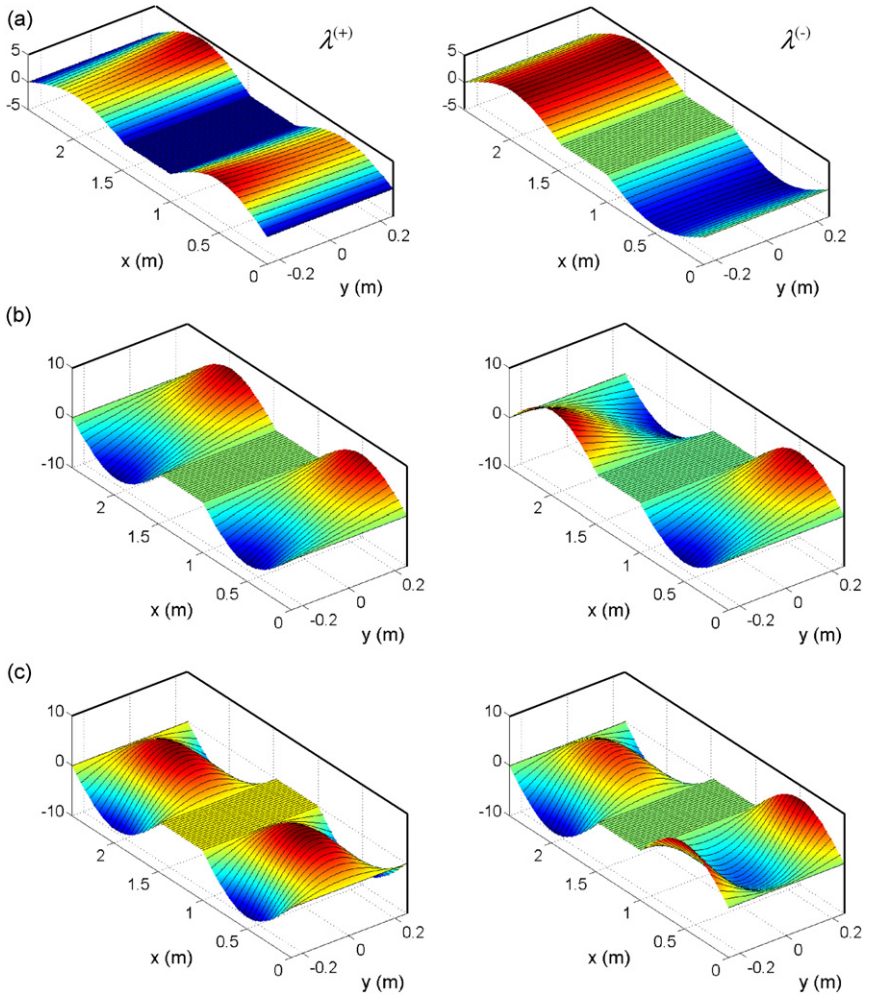

Fig. 5. Examples of symmetric (left) and anti-symmetric (right) modes, where $L_1=L_3=1.0$ m, $L_y=0.5$ m, $h=100$ μm, $R_c=0.15$ m, $\theta=180^\circ$ and $T=150$ N/m. (a) $m=1$, $n=\pm0$, $\lambda^{(+)}=103.03$ rad/s and $\lambda^{(-)}=103.02$ rad/s; (b) $m=1$, $n=\pm1$, $\lambda^{(+)}=103.04$ rad/s and $\lambda^{(-)}=103.03$ rad/s; (c) $m=1$, $n=\pm2$, $\lambda^{(+)}=103.20$ rad/s and $\lambda^{(-)}=103.18$ rad/s.

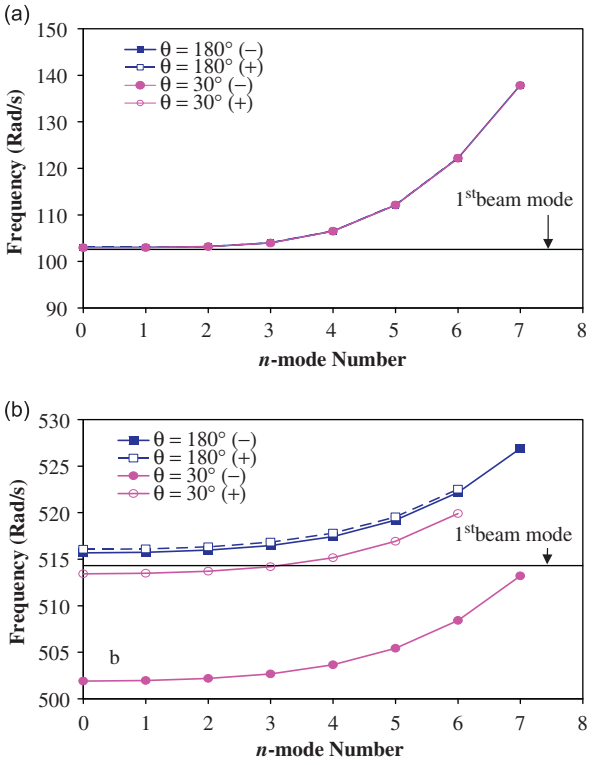

Fig. 6. Effect of wrap angle (θ) and unwrapped length (L_1, L_3). The first 15 lateral (n) frequencies (for m=1) for L_y=0.5 m, h=100 μm, R_c=0.15 m, θ=30, 180° and T=150 N/m: (a) L_1=L_3=1 m and (b) L_1=L_3=0.2 m.

5.1. *Effect of helix angle (β)*

Wrapping a plate in a helical manner around a cylinder alters the dimensions of its flat segments, which become trapezoids for $\beta > 0$, as shown in Fig. 1. This naturally implies that the lengths of the free edges change with respect to β=0 case. When the helix angle is applied half-way across the width of the plate (y=0), as shown in Fig. 1c, the two rectangular flat segments of the wrapped plate become two trapezoidal flat segments, with free-edge lengths of $L_1 \pm \Delta L$ and $L_3 \pm \Delta L$, where $\Delta L = L_y \tan(\beta)/2$. In addition, the shell stiffness also depends on the helical wrap, as shown in Eq. (9). These two effects result in changing the dynamic response. The effect of helical wrap was investigated for helix angles of β=5°, 10°, 22.5° and 45° for a system with dimensions 1 □ 0.5 m when β=0.

The change of the lengths of the free edges, due to helical wrap, results in making the shorter edge of the plate stiffer, while making the longer edge more compliant, relative to the rectangular plate. This variation of stiffness results in significant modifications of the mode shapes of the lateral (n) modes as shown in Fig. 7. The changes are characterized by the localized excitation of the longer, more compliant edge with negligibly small excitation of the shorter, stiffer edge. While specific mode shapes correspond to distinct eigenvalues, the mode shapes cannot be easily identified by the mode numbers in the classical sense. For example, while the first modes shown in Figs. 7b–d are called m=1, n=0, here, a truly n=0 does not exist in the helically wrapped cases, and the lowest modes involve excitation of both x- and y-direction modes; or, considering the m=1, n=3 cases, three inflection points are observed in the lateral direction for β=0° and 10°, but four are seen in the β=22.5° and 45° cases. The mode shapes for higher eigenvalues (i.e., higher n-values) extend across the width of the plate, whereas those for the lower n-values predominantly excite the compliant edge, as shown in Fig. 7.

Comparing the natural frequencies of the helically wrapped plates to the β=0 case, the effect of the helical wrap could be further analyzed. Fig. 8 shows the percentage of frequency change with respect to the β=0 case as a function mode number for different helix angles. Note that positive change corresponds to higher natural frequencies compared to the β=0 case, and vice versa. This figure shows that for the smaller helical angles, the natural frequencies increase with respect to β=0 case, indicating that the stiffer (shorter) side of the plate dominates the response. It is seen that the difference in natural frequencies for higher lateral (n) modes reaches a peak for each helix angle. The difference then decreases and approaches zero. The peak coincides with a lateral vibration mode extending across the entire width of the plate. As the helical wrap angle is increased, the longer, more compliant half of the trapezoidal plate dominates the natural frequency response, leading to lower natural frequencies; it is seen that the frequency change can be on the order of 20% of the β=0 case.

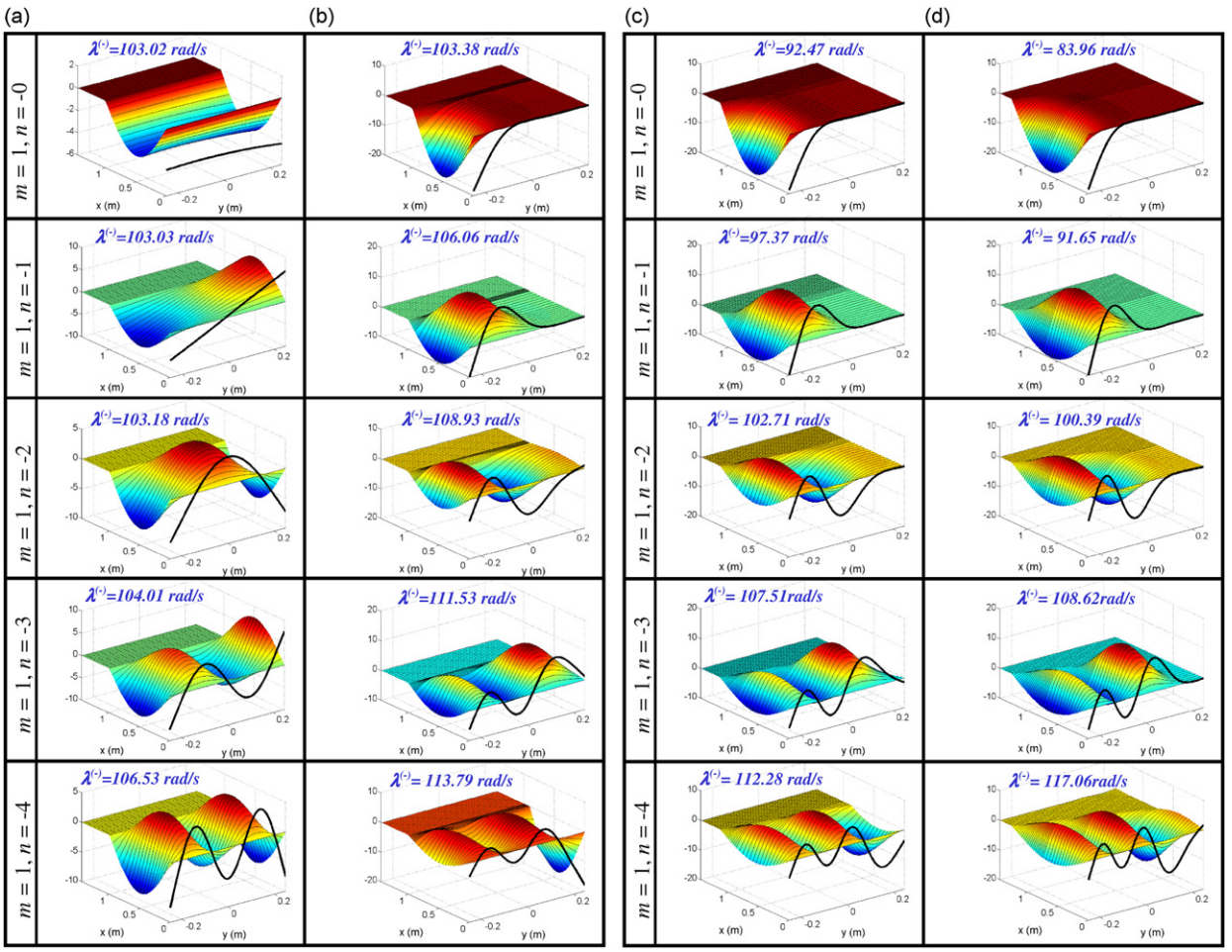

Fig. 7. Computed mode shapes of the helically wrapped plate for β=0°, 10°, 25° and 45°, for L_1=L_3=1 m, L_y=0.5 m, h=100 μm, R_c=0.15 m, θ=180°, and T=150 N/m. Note that only one half of the plate is shown, due to symmetry. (a) β=0°, (b) β=10°, (c) β=22.5° and (d) β=45°.

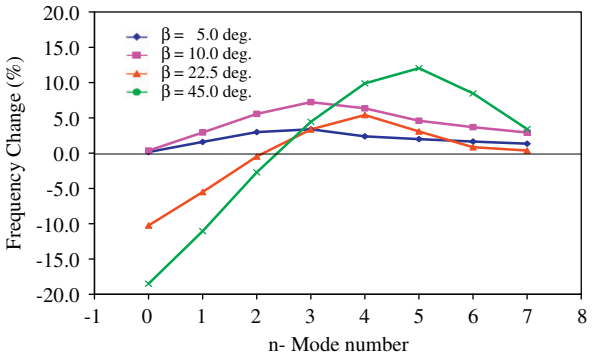

Fig. 8. Frequency change of (m=1, $n^{(-)}$) modes as a function of helical angle. Initial rectangular plate L_1=L_3=1 m, L_y=0.5 m, h=100 μm, R_c=0.15 m, T=150 N/m, θ=180°. Helical angle varied β=5°, 10°, 22.5°, and 45°.

5.2. *Effects of tension, T and helix angle β*

The web tension is expected to have a strong effect on the magnitude of the natural frequencies, as it provides a resistive (restoring force) for out-of-plane web deflection. It is well known that this added stiffness increases the natural frequencies in strings (higher m-modes at higher frequencies). We find that, for the parameters considered here, increasing

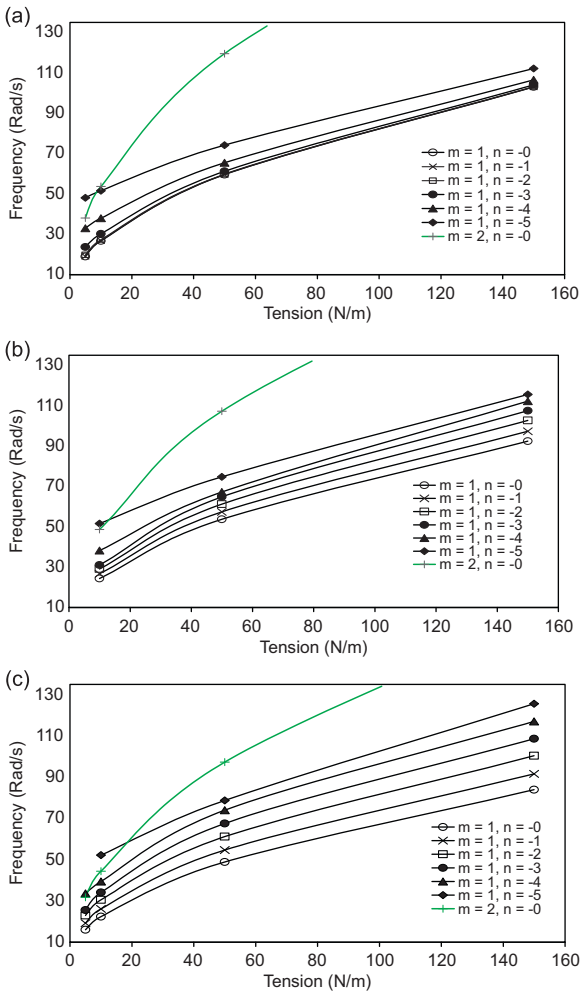

Fig. 9. Effect of helix angle (β) on frequency clustering. Frequencies of first 6 anti-symmetric lateral (n) modes with m=1, for a case where L_1=L_3=1 m, L_y=0.5 m, h=100 μm, R_c=0.15 m, θ=180° and varying tensions. (a) β=0°; (b) β=22.5°; (c) β=45°.

tension also retards the appearance of higher lateral (n) modes. The magnitude of this effect varies depending on the other design parameters, but the increase in frequency applies to all cases. The effects of web tension and helical angle β on the first six anti-symmetric modes are presented in Fig. 9. In Fig. 9a, where β=0, the lateral (n) modes cluster about the more dominant longitudinal (m) mode in a narrow frequency band, especially for m=1, n=0−3. This type of clustering has also been reported by Raman et al. [4]. The clustering of the lateral (n) modes increases for higher tension as higher-order longitudinal (m) modes are suppressed. Fig. 9b and c, where β=22.5° and 45°, respectively, show that for higher helical angles, the clustering effect decreases as the frequencies of higher lateral (n) modes become more unique.

5.3. *Effects of cylinder radius, R_c*

The radius of the cylinder (e.g. turn-bar), R_c, influences the shell stiffness, $D_t(\cos^2\beta+\nu\sin^2\beta\cos^2\beta)/R_c$, of the curved region of the wrapped plate. The effects of the guide radius on the lowest natural frequencies of the system are investigated for R_c=5 and 30 cm at β=45°. No appreciable change can be seen in Fig. 10, where the first five frequencies for both guide radii are plotted. This indicates that, as far as the low end of the frequency range is concerned, the curved section of the shell is effective in serving as a fixed-boundary.

5.4. *Effect of plate width, L_y and wrap angle, θ*

The effects of the width, L_y, of the wrapped plate and the wrap angle, θ, on the natural frequencies is investigated for L_y=0.25 and 0.5 m, and θ=30° and 180°. The eigenvalues for modes m=1 and n= ±0, ±1, …, ±6, −7 are given for θ=180° and 30° in Fig. 11a and b, respectively. When the wrap angle is large (θ=180°), Fig. 11a shows that the eigenvalues of the

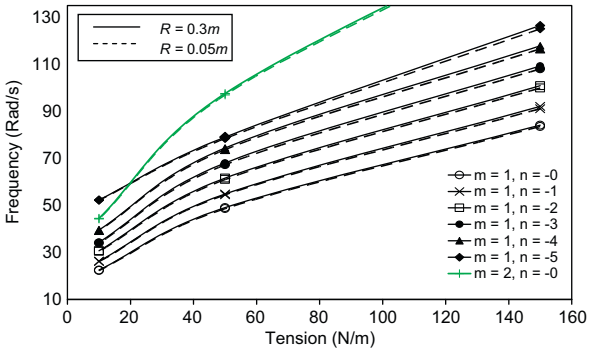

Fig. 10. Effect of radius (R_c) on frequencies of first 6 anti-symmetric lateral (n) modes with m=1. Plate parameters are L_1=L_3=1 m, L_y=0.5 m, h=100 μm, R_c=0.05 m and 0.3 m, θ=180°, β=45° and varying tensions.

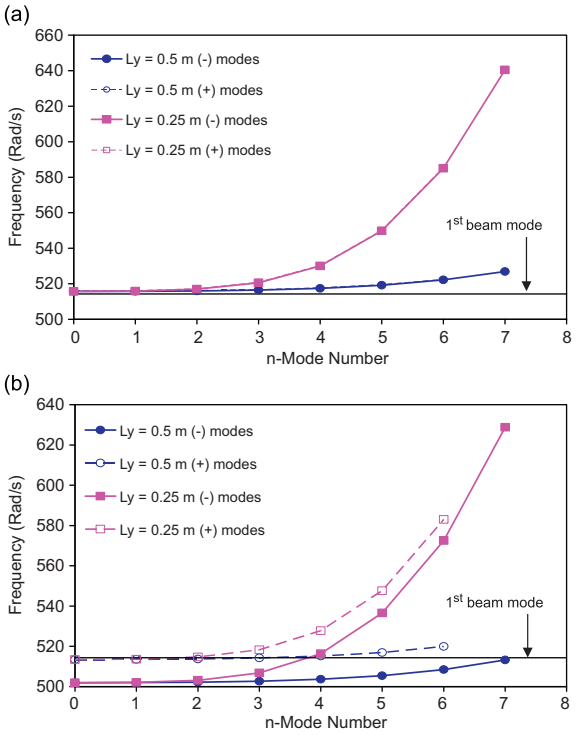

Fig. 11. Effect of width (L_y) and wrap angle (θ) on natural frequencies for a case where L_1=L_3=0.2 m, L_y=0.25 and 0.5 m, h=100 μm, R_c=0.15 m and T=150 N/m. (a) θ=180° and (b) θ=30°.

symmetric and anti-symmetric modes are nearly coincident for both wide and the narrow webs. However, for the case of smaller wrap angle (θ=30°) the eigenvalues of the symmetric and anti-symmetric modes are more distinct. This is attributed to the wrap region providing a lower effective stiffness for the lower wrap angle.

Both of Fig. 11a, b also show that the narrower plates have higher eigenvalues. This indicates that the lateral stiffness of the plate increases for narrower plates, in this system. Finally, these figures also show that the eigenvalues are very close to one another at the lower n-modes, for the two plate widths, and they become more distinct at higher n-modes. This effect is attributed to the fact that the lower n-modes are affected by the plate tension, where the longitudinal (m) mode is more dominant. For the higher n-modes the effects of bending stiffness and lateral geometric stiffness take over, and the eigenvalues are separated as shown.

In summary, Fig. 11 shows the effects of the width and wrap angle on the ability of the plate/shell boundary to act as a stiff constraint. It is shown that by reducing the wrap angle, and/or by using a wider web the stiffness of the plate/shell boundary is weakened. This leads to a separation of the frequencies of the symmetric and anti-symmetric modes, as shown in Fig. 11b. Also note that the eigenmodes associated with the lower wrap angle have lower natural frequencies to excite the non-wrapped sections.

6. Summary and conclusions

In this work, free vibration analysis of a thin tensioned plate, wrapped around a cylindrical surface in a helical manner is presented. The system represents a flexible web wrapped around a turn-bar, which provides non-contact support. The eigenvalue problem was solved numerically where the spatial modes were obtained by the finite element method. Effects of the parameters such as tension, cylinder radius, longitudinal wrap angle, plate width, lengths of non-wrapped segments and helical wrap angle were studied.

When the plate is wrapped symmetrically about the cylinder, eigenmodes with the same mode numbers are observed in symmetric and anti-symmetric fashion about the center of the plate. It was shown that the plate/shell boundary of the wrapped plate effectively acts like support. The "stiffness" of this support depends on the problem parameters, where narrower plates, smaller cylinders, and shorter free span lengths cause an increase in the effective stiffness of the wrapped segment.

It was seen that in the case of straight wrapping (β=0) the free edges of the plate cause frequency clustering of the lateral modes about the dominant longitudinal mode, as also described by Raman et al. [4]. It was shown that increasing the helix angle reduces the shell stiffness and modifies the effective stiffness of the lateral edges of the flat segments of the wrapped plate. As a result, the vibration modes transition the excitation from the more compliant (i.e. longer) edge to the stiffer edge. Overall, it was seen that the first natural frequency is reduced at large helix angles, and the frequency clustering effect observed for straight wrap case is diminished. In general, higher tension suppresses the appearance of higher longitudinal modes and causes increased frequency clustering. These results are significant in the design of web handling systems where excessive vibrations can cause permanent damage. However, in order to analyze the frequency effects in high-transport speed web handling systems the gyroscopic acceleration effects should be included in the analysis.

Acknowledgements

The authors would like to thank Mr. James Masters (CD-Adapco, Melville, NY) who developed the original version of the finite element program that eventually lead to this work, and to Dr. Kevin Cole (Optimation Technology Inc., Rush, NY) for providing Fig. 1a, and helpful discussions over the years.

Appendix: Finite element approach

In this appendix, the shape functions, matrices and vectors utilized in the finite element approach of the vibration analysis are given. The following shape functions were used to interpolate a four-node quadrilateral element for both nodal coordinates and nodal degrees of freedom in what is known as an isoparametric formulation:

$$N_1=\frac{1}{4}(1-\xi)(1-\eta)\quad(a)\quad N_2=\frac{1}{4}(1+\xi)(1-\eta)\quad(b)$$

$$N_3=\frac{1}{4}(1+\xi)(1+\eta)\quad(c)\quad N_4=\frac{1}{4}(1-\xi)(1+\eta)\quad(d)\tag{A1}$$

These shape functions are expressed in natural coordinates in order to accommodate non-rectangular element deformations. Since Mindlin based elements are used, C^0 continuous shape functions are permitted, but it should be noted that in order to alleviate the locking effect the shear stresses need to be interpolated differently.

The bending shape function derivative matrix, $\mathbf{B}_b$, is given as follows:

$$\mathbf{B}_b=\begin{bmatrix}\frac{\partial N_i}{\partial\xi} & 0 & 0\\ 0 & \frac{\partial N_i}{\partial\eta} & 0\\ \frac{\partial N_i}{\partial\eta} & \frac{\partial N_i}{\partial\xi} & 0\end{bmatrix}\tag{A2}$$

$\mathbf{B}_s$ is the shear stiffness shape function derivative matrix:

$$\mathbf{B}_s=\begin{bmatrix}N_i & 0 & \frac{\partial N_i}{\partial\xi}\\ 0 & N_i & \frac{\partial N_i}{\partial\eta}\end{bmatrix}\tag{A3}$$

Note, this matrix is modified to $\mathbf{B}_s'$, in order to eliminate the shear locking effect. This is done following the procedure outlined by Donea and Lamain [25]. The final result is a new shear energy shape function derivative matrix:

$$\mathbf{B}_s'=\begin{bmatrix}M_i^{\theta} & M_i^{\phi} & N_{i,\xi}\\ L_i^{\xi} & L_i^{\phi} & N_{i,\eta}\end{bmatrix}\tag{A4}$$

The components are found using the following vectors:

$$\begin{Bmatrix} M_1^\alpha \\ M_2^\alpha \\ M_3^\alpha \\ M_4^\alpha \end{Bmatrix} = \frac{1}{8|J|}\begin{bmatrix} y_{,\eta} & 0 & -y_{,\xi} & 0 \\ y_{,\eta} & 0 & 0 & -y_{,\xi} \\ 0 & y_{,\eta} & 0 & -y_{,\xi} \\ 0 & y_{,\eta} & -y_{,\xi} & 0 \end{bmatrix}\begin{Bmatrix} (1-\eta)(Z_2-Z_1) \\ (1+\eta)(Z_3-Z_4) \\ (1-\xi)(Z_4-Z_1) \\ (1+\xi)(Z_3-Z_2) \end{Bmatrix} \quad (a) \tag{A5}$$

$$\begin{Bmatrix} L_1^\alpha \\ L_2^\alpha \\ L_3^\alpha \\ L_4^\alpha \end{Bmatrix} = \frac{1}{8|J|}\begin{bmatrix} -x_{,\eta} & 0 & x_{,\xi} & 0 \\ -x_{,\eta} & 0 & 0 & x_{,\xi} \\ 0 & -x_{,\eta} & 0 & x_{,\xi} \\ 0 & -x_{,\eta} & x_{,\xi} & 0 \end{bmatrix}\begin{Bmatrix} (1-\eta)(Z_2-Z_1) \\ (1+\eta)(Z_3-Z_4) \\ (1-\xi)(Z_4-Z_1) \\ (1+\xi)(Z_3-Z_2) \end{Bmatrix} \quad (b)$$

where $Z=x$, for $\alpha=\theta$ and $Z=y$, for $\alpha=\phi$. x and y are the global coordinates of the node and, $|J|$, is the determinant of the Jacobian matrix [30]. The shape function matrices $\mathbf{N}_d$ and $\mathbf{N}_\Phi$ are defined as follows:

$$\mathbf{N}_d = \begin{bmatrix} 0 & 0 & N_i \end{bmatrix} \tag{A6}$$

$$\mathbf{N}_\Phi = \begin{bmatrix} 0 & 0 & 0 \\ 0 & 0 & 0 \\ 0 & 0 & N_i \end{bmatrix} \tag{A7}$$

Both of the above shape functions isolate the transverse deflection. The shape function derivative matrix, $\mathbf{B}_\sigma$, is defined as follows:

$$\mathbf{B}_\sigma = \begin{bmatrix} 0 & 0 & \dfrac{\partial N_i}{\partial \xi} \end{bmatrix} \tag{A8}$$

The nodal load vector, $\mathbf{\Theta}$, is defined as follows:

$$\mathbf{\Theta}^{\mathrm{T}} = \begin{Bmatrix} 0 & 0 & p_i \end{Bmatrix} \tag{A9}$$

where p_i is the local applied pressure. Note that the nodal moments are neglected from this nodal load vector.

The element stiffness, $\mathbf{k}^{(e)}$, is the sum of bending, transverse shear, curvature and tension components, defined as follows:

$$\mathbf{k}_b = \int_A \mathbf{B}_b^{\mathrm{T}}\mathbf{D}_b\mathbf{B}_b J\,\mathrm{d}\xi\,\mathrm{d}\eta \tag{A10}$$

$$\mathbf{k}_s = \int_A \mathbf{B}_s'^{\mathrm{T}}\mathbf{D}_s\mathbf{B}'_s J\,d\xi\,d\eta \tag{A11}$$

$$\mathbf{k}_d = \frac{1}{2}D_t\int_A (b_{xx}^2 + \nu b_{xx}b_{yy})\mathbf{N}_d^{\mathrm{T}}\mathbf{N}_d J\,d\xi\,d\eta \tag{A12}$$

$$\mathbf{k}_\sigma = T_x\int_A \mathbf{B}_\sigma^{\mathrm{T}}\mathbf{B}_\sigma J\,d\xi\,d\eta \tag{A13}$$

where J is the Jacobian. The vectors, $\mathbf{r}_\Phi$ and $\mathbf{r}_\sigma$ represent external load and the belt-wrap pressure acting on the element nodes, respectively,

$$\mathbf{r}_\Phi = \int_A \mathbf{N}_\Phi^{\mathrm{T}}\mathbf{N}_\Phi\mathbf{\Theta}J\,d\xi\,d\eta \tag{A14}$$

$$\mathbf{r}_\sigma = T_x\int_A b_{xx}\mathbf{N}_d^{\mathrm{T}}J\,d\xi\,d\eta \tag{A15}$$

The integrals are evaluated by using the Gauss quadrature technique with sampling points at $\xi,\eta = \pm 1/\sqrt{3}$ [18].

References

[1] S. Müftü, Mechanics of thin, flexible translating media and their interactions with surrounding air, *Japan Society Mechanical Engineering International Journal, Series C* 48 (2005) 329.

[2] S. Müftü, K.A. Cole, The fluid/structure interaction of a thin flexible cylindrical web supported by an air cushion, *Journal of Fluids and Structures* 13 (1999) 681.

[3] S. Müftü, Mechanics of a thin, tensioned-shell, wrapped helically around a turn-bar, *Journal of Fluids and Structures* 23 (2007) 767.

[4] A. Raman, K. Wolf, P. Hagedorn, Observations on the vibrations of paper webs, in: *Proceeding of IWEB Conference, Oklahoma State University*, 2001.

[5] A.G. Ulsoy, Coupling between spans in the vibration of axially moving materials, *Journal of Vibration and Acoustics* 108 (1986) 207.

[6] C.S. Huang, A.W. Leissa, M.J. Chang, Vibrations of skewed cantilever triangular, trapezoidal parallelogram Mindlin plates with considering corner stress singularites, *International Journal for Numerical Methods in Engineering* 63 (2005) 1789.

[7] I. Chopra, S. Durvasula, Vibration of simply-supported trapezoidal plates. I—symmetric trapezoids, *Journal of Sound and Vibration* 19 (1971) 379.

[8] I. Chopra, S. Durvasula, Vibration of simply-supported trapezoidal plates. II—unsymmetric trapezoids, *Journal of Sound and Vibration* 20 (1972) 125.
[9] M.S. Qatu, N.A. Jaber, A.W. Leissa, Natural frequencies for completely free trapezoidal plates, *Journal of Sound and Vibration* 167 (1991) 183.
[10] K.M. Liew, K.Y. Lam, A Rayleigh–Ritz approach to transverse vibration of isotropic and anisotropic trapezoidal plates using orthogonal plate functions, *International Journal of Solids and Structures* 27 (1991) 189.
[11] J.A. Wickert, C.D. Mote Jr., Classical vibration analysis of axially moving continua, *Journal of Applied Mechanics* 57 (1990) 738.
[12] V. Kartik, J.A. Wickert, Parametric instability of a traveling plate partially supported by a laterally moving elastic foundation, *Journal of Vibration and Acoustics* 130 (2008).
[13] A. Pramilla, Natural frequencies of a submerged axially moving band, *Journal of Sound and Vibration* 113 (1987) 198.
[14] P.M.J. Rongen, On numerical solutions of the instationary 2D foil bearing problem, *Tribology and Mechanics of Magnetic Recording Systems, Society of Tribologists and Lubrication Engineers, Special Publication, SP-29* (1990) 130.
[15] P.M.J. Rongen, Finite Element Analysis of the Tape Scanner Interface in Helical Scan Recording, Ph.D. Dissertation, Technical University of Eindhoven, The Netherlands, 1994.
[16] F.I. Niordson, *Shell Theory*, North-Holland, Amsterdam, 1985.
[17] L.H. Donnell, *Beams, Plates and Shells*, McGraw-Hill, New York, 1976.
[18] R. Cook, D. Malkus, M. Plesha, R. Witt, *Concepts and Application of Finite Elements Analysis*, John Wiley & Sons, New York, USA, 2002.
[19] O.C. Zienkiewicz, E. Hinton, Reduced integration, function smoothing and non-conformity in finite element analysis (with special reference to thick plates), *Journal of the Franklin Institute* 302 (1976) 443.
[20] O.C. Zienkiewicz, J. Bauer, K. Morgan, E. Onate, A simple and efficient element for axisymmetric shells, *International Journal for Numerical Methods in Engineering* 11 (1977) 1545.
[21] T.J.R. Hughes, M. Cohen, M. Haroun, Reduced and selective integration techniques in the finite element analysis of plates, *Nuclear Engineering and Design* 46 (1978) 203.
[22] T.J.R. Hughes, R.L. Taylor, W. Kanoknukulchai, A simple and efficient finite element for plate bending, *International Journal for Numerical Methods in Engineering* 11 (1977) 1529.
[23] S.W. Lee, C. Wong, Mixed formulation finite elements for Mindlin theory plate bending, *International Journal for Numerical Methods in Engineering* 18 (1982) 1297.
[24] K.J. Bathe, E.N. Dvorkin, Short communication, a four-node plate bending element based on Mindlin/Reissner plate theory and a mixed interpolation, *International Journal for Numerical Methods in Engineering* 21 (1985) 367.
[25] J. Donea, L.G. Lamain, A modified representation of transverse shear in C^0 quadrilateral plate elements, *Computer Methods in Applied Mechanics and Engineering* 63 (1987) 183.
[26] P.M. Pinsky, R.V. Jasti, A mixed finite element formulation for Reissner–Mindlin plates based on the use of bubble functions, *International Journal for Numerical Methods in Engineering* 28 (1989) 1677.
[27] G. Shi, G.Z. Voyiadjis, Simple and efficient shear flexible two-node arch/beam and four-node cylindrical shell/plate finite elements, *International Journal for Numerical Methods in Engineering* 31 (1991) 759.
[28] S.H. Kim, C.K. Choi, Improvement of quadratic finite element for Mindlin plate bending, *International Journal for Numerical Methods in Engineering* 34 (1992) 197.
[29] L.M. Bucalem, K.J. Bathe, Higher-order MITC general shell elements, *International Journal for Numerical Methods in Engineering* 36 (1993) 3729.
[30] K.J. Bathe, *Finite Element Procedures*, Prentice-Hall, Inc., New Jersey, 1996.
[31] O. Polit, M. Touratier, P. Lory, A new eight-node quadrilateral shear-bending plate finite element, *International Journal for Numerical Methods in Engineering* 37 (1994) 387.
[32] K.U. Bletzinger, M. Bischoff, E. Ramm, A unified approach for shear-locking free triangular and rectangular shell finite elements, *Computers and Structures* 75 (2000) 321.
[33] R.J. Marczak, A.M. Awruch, A locking-free three-node shell finite element formulation. Computational Mechanics, New Trends and Applications (1998).
[34] H.R.H. Kabir, A shear-locking free isoparametric three-node triangular finite element for moderately thick and thin plates, *International Journal for Numerical Methods in Engineering* 35 (1992) 503.
[35] R.C. Averill, J.N. Reddy, An assessment of four-noded plate finite elements based on a generalized third-order theory, *International Journal for Numerical Methods in Engineering* 33 (1992) 1553.
[36] X. Wang, Numerical analysis of moving orthotropic thin plates, *Computers and Structures* 70 (1999) 467.
[37] LAPACK Users Guide from 〈http://www.netlib.org/lapack/faq.html〉.
[38] R. Sundaram, R.C. Benson, Personal communication, 1989.
[39] E. Lopez, Vibrations and Fluid Structure Interactions in Web Handling Systems, Ph.D. Thesis, Northeastern University, Boston, MA 02115, 2009.